A power and energy procedure in operating photovoltaic systems to quantify the losses according to the causes

A Power and Energy Procedure in Operating Photovoltaic Systems to Quantify the Losses According to the Causes

F. Spertino[1], A. Ciocia[1], P. Di Leo[1], R. Tommasini[1], I. Berardone[2], M. Corrado[2], A. Infuso[2], M. Paggi[3]

[1] Politecnico di Torino, Energy Department, [2] Department of Structural, Geotechnical and Building Engineering, corso Duca degli Abruzzi, 24 – 10129 Torino, Italy

[3] IMT Institute for Advanced Studies Lucca, Piazza S. Francesco 19, I-55100, Lucca, Italy

Corresponding author:

Filippo Spertino

Politecnico di Torino, Energy Department

corso Duca degli Abruzzi 24, I-10129 Torino, Italy

e-mail filippo.spertino@polito.it

Abstract: Recently, after high feed-in tariffs in Italy, retroactive cuts in the energy payments have generated economic concern about several grid-connected photovoltaic (PV) systems with poor performance. In this paper the proposed procedure suggests some rules for determining the sources

of losses and thus minimizing poor performance in the energy production. The on-site field inspection, the identification of the irradiance sensors, as close as possible the PV system, and the assessment of energy production are three preliminary steps which do not require experimental tests. The fourth step is to test the arrays of PV modules on-site. The fifth step is to test only the PV strings or single modules belonging to arrays with poor performance (e.g., mismatch of current-voltage curves). The sixth step is to use the thermo-graphic camera and the electroluminescence at the PV-module level. The seventh step is to monitor the DC racks of each inverter or the individual inverter, if equipped with only one Maximum Power Point Tracker (MPPT). Experimental results on real PV systems show the effectiveness of this procedure.

Keywords: solar cell *I-V* mismatch; PV testing; electroluminescence; grid-connected PV system.

Nomenclature

Acronyms

ADAS	Automatic Data Acquisition System
BIPV	Building Integrated PhotoVoltaic
GMPV	Ground Mounted PhotoVoltaic
EL	ElectroLuminescence
IR	InfraRed
MPPT	Maximum Power Point Tracker
m-Si	mono-crystalline Silicon
p-Si	poly-crystalline Silicon
PCU	Power Conditioning Unit
PID	Potential Induced Degradation
PV	PhotoVoltaic
RMS	Root Mean Square
STC	Standard Test Conditions

Symbol Description

I-V	current-voltage
E_{AC_p}	predicted daily energy delivered to the AC grid (kWh)
E_{AC_m}	monitored daily energy delivered to the AC grid (kWh)
$\varepsilon_{p\text{-}m}$	relative deviation between E_{AC_p} and E_{AC_m}
$P_{p,k}$	*k-th* peak power of PV array (kWp)
$Y_{r,k}$	*k-th* reference yield on the plane of array (h/year)
η_{therm}	thermal efficiency of the array
γ	maximum power temperature coefficient of PV modules (pu/°C)
T_C	cell temperature (°C)
ΔT	deviation of cell temperature from the STC value (°C)
η_{array}	efficiency due to non-thermal losses of the PV array
η_{shade}	efficiency due to shading effect on the PV array
η_{PCU}	efficiency of PCU
$P_{M,k}$	maximum power of the *k*-th module in stand-alone operation (kW)
$P_{M,array}$	maximum power at *STC* after array connection (kW)
$\ell_{mis}^{(array)}$	relative power losses due to I-V mismatch in a PV array
G	solar irradiance (W/m^2)
T_a	ambient temperature (°C)
I_{sc}	short circuit current (A)
V_{oc}	open circuit voltage of PV generator (V)
P_M	maximum power of PV generator (kW)
FF	fill factor
P_{mpp}	maximum power after irradiance and temperature corrections at *STC* (kW or W)
I_{mpp}	current at maximum power after irradiance and temperature corrections at *STC* (A)
V_{mpp}	voltage at maximum power after irradiance and temperature corrections at *STC* (V)
ΔI_{mpp}	current deviation at MPP with respect to datasheet

ΔV_{mpp}	voltage deviation at MPP with respect to datasheet
I_{ph}	photovoltaic current of solar-cell equivalent circuit (A)
m	junction quality factor of solar-cell equivalent circuit
I_0	dark saturation current of solar-cell equivalent circuit (μA)
R_s	series resistance of solar-cell equivalent circuit (Ω)
R_{sh}	shunt resistance of solar-cell equivalent circuit (Ω)

1. INTRODUCTION

Today, after years of generous feed-in tariff with the consequent deployment of grid-connected photovoltaic (PV) systems, a new phase occurs in Italy, where a retroactive cut is in force for the amount paid on energy production [1]. PV systems, characterized by sufficient energy production in the previous framework, are no more adequate to produce profits for the investors within the new regulations. Hence, it is important to evaluate the losses in the energy production according to the different causes. The Building Integrated PhotoVoltaic (BIPV) systems are affected by a number of worsening phenomena [2] such as: shading effects generated by near obstacles; thermal gradients from lower parts to upper parts of the roofs; impact of dirt for pollution; non-optimal exposition to the Sun. But the most of photovoltaic capacity is composed of large PV systems mounted at ground level. These plants are characterized by: partial shading on the PV modules, if the mutual distances among the mounting structures were reduced to increase the land utilization; placement of PV modules too close to the ground with the inherent effect of dampness and dirt accumulation on the frame. As previously written, in Italy a simultaneous condition of high feed-in tariff and low price of PV modules triggered the installation of ≈11 GWp in 2011. The supply of the components, PV modules and Power Conditioning Units (PCUs), was difficult with many delays. The need for speedy design and installation sometimes caused drawbacks summarized in the following bullet points:

- The mismatch between an optimal design and the installation has provoked the possibility of:
  1. Current-voltage (*I-V*) mismatch in the case of slightly different peak power in series connected

modules of the strings connected in parallel inside a PV array.

2. Partial shading on the PV modules.
3. A non-optimal match between the peak power of the PV array and the rated power of the power conditioning unit (many times named “inverter”).
4. Cracks in silicon solar cells due to improper handling during transportation and installation.

- The use of components, such as PV modules and PCUs, which are not of the best manufacturing quality and may exhibit underperformance (i.e., mismatch in the electrical parameters of the PV modules) during the outdoor operation, but are readily available on the market at the moment of the installation.

Most of the underperformance observed in the field is due to PV modules rather than to the other components. Multiple types of degradation [3], such as shunt defects and micro-cracks in solar cells, Potential Induced Degradation (PID), visible snail tracks were noticed in the tested PV modules.

Therefore, the check of energy production is of paramount importance to guarantee investors their monetary return. Indeed, the maintenance costs, related to the monitoring of degradation mechanisms and the replacement of failed PV modules, are not taken into account in the business plans. The Standard [4] is a reference in this topic: it describes “the minimum commissioning tests, inspection criteria and documentation expected to verify the safe installation and correct operation of the system”. However, the goal of current paper is to define a reasonable procedure, in terms of minimum type and number of tests and thus minimum duration (a few days), in order to identify the sources of poor performance and to solve or mitigate their negative effects. Such a procedure is based on experimental tests, partly on the PV-system site and partly in laboratory, and the suitable data processing, both before the experiments and after them.

2. POWER AND ENERGY PROCEDURE

In this section the peculiarities of the proposed procedure are presented with respect to the Standard [4]. Differently from the above mentioned Standard, the new procedure does not include safety tests

as the continuity of protective grounding conductors and the PV-array insulation resistance tests. The main reason is that these tests negligibly affect the energy production and PCUs are normally equipped with detectors of insulation resistance. In addition, the new procedure permits an easy identification of the underperformance, thanks to the comparison of the monitored energy production with the expected productivity based on a suitable model. Then, as a first experimental test, it is recommended to distinguish very quickly portions (arrays) of the PV field, in which no further experimental tests are required (acceptable performance) or, on the contrary, deep analysis is required at string and PV module levels. This ability, which minimizes the lost production during the disconnection of PV modules to carry out their tests (<1 s per each test), is given by the *I-V* curve measurement at level of PV array without the typical size limits of the commercial instrumentations, i.e., ≤100 kWp as written in [5],[6]. Moreover, the uncertainty of the measurements is guaranteed by repetitive calibrations of the Automatic Data Acquisition System (ADAS) used in the on-site testing. Even if this reference Standard includes the InfraRed (IR) camera inspection to check thermal problems, the new procedure involves the electroluminescence test which is of primary importance to understand the causes of defects in the solar cells of PV modules. A detailed description of this procedure, with top-down approach, is outlined as follows:

A. *On-site field inspection* regarding the weak points described in the bullet points of Introduction, in comparison with an optimal design. E.g., a check of electrical parameters for DC/AC cables and grid transformer, a study of shading pattern, if present, are performed. The beginning and the end of the shadows projected on the PV strings are calculated. If one PV module inside a string is shaded, the current is generated, with a pessimistic assumption, only by the diffuse component of irradiance. This step includes also the confirmation of the electrical parameters of the utility grid at the interface protections from historical data to assess the availability of the grid voltage.
B. *Identification of the irradiance sensors* for the PV system under test; obviously, the irradiance and temperature sensors must be calibrated with respect to the national standards. Many times the PV plants are equipped with irradiance sensors, made of the same material of the PV modules. The

advantages of the solar cell sensors are their cheap price, long term calibrations and a fast response versus rapid changes in irradiance. Nevertheless, their main drawback is a so low accuracy that the assessment of the PV plant efficiency is often unreliable. Thus, the best solution is represented by pyranometers, calibrated year by year, which measure the global irradiation on the plane of array. However, in the BIPV systems, where the tilt and azimuth angles are multiple, this solution implies unacceptable costs (ten times the cost of a reference solar cell per each pyranometer). As a consequence, the viable solution is represented by the horizontal irradiation data with typical uncertainty ≈±2% from meteorological stations in the PV site or in the surrounding neighbourhood.

C. *Assessment of the energy production* to compare the experimental data from the on-site PV monitoring system with the reference production obtained by a suitable model. The calculation of their deviations is needed for the next analysis devoted to the quantification of the sources of losses. The reference production is computed by the Italian standard [7] with a summation formula, in which the number of PV arrays N_a is the upper bound:

$$E_{AC\_p} = \sum_{k=1}^{N_a} P_{p,k} \cdot Y_{r,k} \cdot \eta_{therm,k} \cdot \eta_{array,k} \cdot \eta_{shade,k} \cdot \eta_{PCU,k} \quad (1)$$

- E_{AC_p} is the predicted daily energy in kWh;
- $P_{p,k}$ is the *k-th* peak power of PV array (kWp);
- $Y_{r,k}$ is the *k-th* reference yield [8] on the plane of array (thanks to calibrated pyranometers);
- $\eta_{therm,k}$ takes into account the temperature losses and it is equal to $(1+\gamma \cdot \Delta T)$, where γ is the thermal coefficient of the PV module maximum power and ΔT is the temperature deviation of the solar cells from the standard value (25 °C);
- $\eta_{array,k}$ represents the non-thermal losses of the PV array, such as DC cables, manufacturing tolerance and I-V mismatch, dirt, glass reflection, etc. It is fixed at 92% by the previous standard [8] for PV modules of recent production with a tolerance = ±3% or less;

- $\eta_{shade,k}$ determines the shading effect on the PV array, simply computed as ratio of the actual energy output to the available energy without shade projected by near obstacles, during reference days in the four seasons;
- $\eta_{PCU,k}$ is a weighted efficiency of PCU in function of the power output [9],[10].

This energy prediction is compared with the monitored value E_{AC_m} (affected by uncertainty, typically of ±1%) by the relative deviation $\varepsilon_{p\text{-}m}$ according to (2).

$$\varepsilon_{p-m} = \frac{E_{AC\_p} - E_{AC\_m}}{E_{AC\_p}} \tag{2}$$

D. *Measurements of I-V Curves* on *PV Arrays* at the actual conditions of irradiance and temperature, with the successive extrapolation at standard test conditions, to determine the real maximum power in outdoor operation. This activity permits to quantify the cable losses (≈1%) by measuring the *I-V* curves at the beginning and at the end of the lines which connect the PV strings to the PCU.

E. *Measurements of I-V Curves on PV Strings and Modules* after the previous measurements needed to discriminate good PV arrays from defective PV arrays. The purpose is to quantify, after the measurement of string *I-V* curves, the impact of mismatch in parallel connection to form a PV array and, after the measurement of module *I-V* curves, the impact of mismatch in series connection to form a string. The *I-V* mismatch is a loss phenomenon strictly linked to the nonlinearity of the *I-V* curves of the PV modules. The connection in series of modules, with different values of current at their maximum power points (MPPs), and the connection in parallel of strings, with different values of voltage at their MPPs, determine noticeable losses in the resulting *I-V* curve of the PV array. Indeed, two or more PV modules can be subject to *I-V* mismatch, even if their peak powers are equal, but with big production tolerance. In practice, it is very hard to achieve a tolerance of maximum power lower than ±3% and the deviations in current and voltage at MPP are still greater with a consequent higher potential of mismatch. Thus, this performance reduction, due to *I-V* mismatch in N_m modules of an array, can be expressed as relative power losses $\ell_{mis}^{(array)}$ (positive sign) [11]:

$$\ell_{mis}^{(array)} = \frac{\sum_{k=1}^{N_m}\left(P_{M,k}\right) - P_{M,array}}{\sum_{k=1}^{N_m}\left(P_{M,k}\right)} \quad (3)$$

$P_{M,k}$ is the *STC* maximum power of the *k*-th module before the connection with the other modules (stand-alone operation) and $P_{M,array}$ is the actual maximum power at *STC* on the resulting *I-V* characteristic after array connection.

F. *Advanced Diagnostic Techniques* for deeper analysis at the PV-module level by using: 1) thermographic camera during the normal operation, in order to detect hot-spot positions and extents, and 2) electroluminescence test. This was carried out in laboratory after disconnection of the module from the electric circuit, in order to determine the type of defects and infer on its origin (e.g., cells with finger interruptions). These techniques are very useful to assess the origin of power losses and electric degradation at the module level. IR thermography is suitable to visualize hot spots and ascertain various types of failures or general malfunctioning of modules. The causes may be: short circuits; massive shunts caused by Potential Induced Degradation (PID) and/or polarization; shading effects; defective cells; delaminated, broken or cracked cells. For the last category of defects, a finer inspection of crack patterns and the understanding of their source can be achieved via the ElectroLuminescence (EL) technique. It is a non-destructive method based on the evaluation of the level of luminescence emitted by silicon, if subjected to a forward bias voltage. Electrically insulated zones or cracks can be identified by their low EL intensity, thus resulting in less bright images. In the present study, PV modules were taken from the field and tested in the laboratory of the Dept. of Structural, Geotechnical and Building Engineering of Politecnico di Torino. They were supplied by a DC bias from the power supply Genesys. EL emission was detected by the digital 12-bit CCD camera pco.1300 solar, with a resolution of 1392×1040 pixels and equipped with the Schneider Kreuznach lens with SWIR coating of 800–1800 nm. To reach a meaningful level of detection, it is essential to maintain a high ratio “signal to noise”, cutting off all possible sources of light. Thus, tests were performed inside a darkroom to avoid any kind of

reflection. By using nearly the maximum aperture of the camera, the focus was adjusted depending on the distance from the module and an exposure time of 5 s was used. A post-processing of the acquired EL images was made by using the CamWare software.

G. *Measurements of the Main PCU Operating Parameters.* In particular, they are the MPPT and DC-AC efficiencies, to calculate the global PCU efficiency, and some power quality indicators about harmonic content and power factor, thanks to daily tests carried out during the field inspection.

3. Application of the Procedure to Real Case Studies

A. On-site Field Inspection

The power and energy procedure has been applied to two multi-megawatt PV plants. The first PV system with 3.3 MWp is ground-mounted (*GMPV*) for power injection into a rural grid, located in southern Italy. The second PV system, with a peak power of 2.5 MWp, is building integrated (*BIPV*) on the roofs of a factory belonging to the food/pharmaceutical sector in northern Italy.

The *GMPV* system includes both PV modules in poly-crystalline silicon (p-Si), accounting for 3 MWp, and the remainder (0.3 MWp) in mono-crystalline silicon (m-Si). Fig. 1 shows two successive rows of PV modules mounted on open structures close to the terrain. They are arranged in PV arrays which supply MPPT racks with 55 kW rated power. Nine 330 kVA inverters with six MPPT racks each convert DC energy into AC energy delivered to the medium voltage grid.

The *BIPV* system includes mainly PV modules in m-Si (2,3 MWp), and a p-Si remainder (0.2 MWp). The power rating of p-Si modules is 230 Wp, while m-Si modules have different peak powers: 240 and 250 Wp; then, they were connected in strings made of 10 modules without the advisable sorting procedure according to the electrical parameters. The strings were connected in parallel (up to 90) to form arrays ≤225 kWp. The manifold architecture of the roofs (seven tilt angles and four azimuth angles) caused the choice of the multi-inverter configuration with different power ratings: three oversized 250-kVA PCUs; eight oversized 125-kVA PCUs; two oversized 80-kVA PCUs; some tens of smaller size PCUs (12-50 kVA).

During the inspection of the *BIPV* plant, it was observed that a remarkable obstacle (Fig. 2 inside the red circle) can put into shade a part of the PV modules. The 3D model of the obstacle (a tower in the factory) in SketchUp with the near roofs, subject to lateral shades of tower, was created to estimate the resulting power losses on the PV modules. In details, the tower is 25-m higher than the roofs, where these PV modules are placed. The tilt of the roof is 6°, whereas the azimuths are -17° (southeastern) and +163° (northwestern). The decrease of productivity is different for each individual string and depends on the position in which it is installed. To carry out daily simulations representative of the yearly behavior, spring, summer and autumn days are chosen: the winter impact is negligible. The Sun-beam evolution is analyzed with respect to the projected shades on the PV modules: 109 strings in different colors in Fig. 3 at right and left sides of the tower. The irradiance profiles, only for 10 strings with SE (left side) and NW (right side) orientations, are shown in Fig. 4, in which the steep increments and decrements represent the end of shadows in the morning and their beginning in the afternoon on the involved strings. PVGIS [12] provides data on global irradiance and diffuse contribution in monthly mean conditions. The diffuse irradiance is considered, if the shadow of the tower covers at least one of the string modules, neglecting the action of the bypass diodes inside the modules with a pessimistic estimation. As main findings of the simulation on a 272-kWp portion of *BIPV* system, the energy losses are ≈6% in spring, ≈9% in summer and ≈3% in autumn (negligible in winter) with respect to the calculation without the shade effect. However, these losses have an impact <1% on yearly basis (0.7%, 1.1% and 0.3% in the three seasons, respectively), taking into account the relative weight (12% of 2.3 MWp) of the PV system portion in the energy production. In addition, other obstacles, as e.g. balustrades and chimneys, provide losses concentrated in winter (it accounts for 9% of the yearly production) with noticeable deviations with respect to energy calculated without shades. Even if the shades have an impact month by month, the energy reduction per year can be estimated within 1—2%.

The confirmation of grid parameters is very important, if the utility grid is weak. The voltage is high, when the load consumption is poor and the PV system injects power into the grid. The availability of

the grid, vs. the yearly 8760 h, may be <95%. In the PV systems under study the availability is >99% and thus no concern arises.

B. Identification of the Irradiance Sensors

A multi-year analysis of monthly irradiations puts into evidence the role of an accurate and local measurement by pyranometers in the framework of the current climate changes. Actually, mutual distances between meteorological station and PV plant higher than 5-10 km and/or the lack of the radiation data for the year under study can cause noticeable errors in the calculation of the performance ratio [13].

In this case, for the *BIPV* system, the closest weather station of the local Agency for Environmental Protection (ARPA) was selected for the horizontal daily irradiation. The related measurements were transferred on the tilted planes of the manifold roofs in the factory. The procedure for the data correction can be carried out by multiple methods, as e.g. the ones proposed in an Italian standard [14], here used, or in [15]. For the *GMPV* system, the local irradiance sensors was calibrated by the authors' pyranometer [6].

C. Assessment of Energy Production

The explained productivity concept was applied to the PV plants under study: the energy production from spring 2011 to autumn 2013 (on hourly basis) was analyzed for the *BIPV* system. Tables I and II summarize the mean results, also in terms of conventional performance ratio and final yield, during 2.5 years. The relative deviations are strongly negative: in average, -20% with estimated uncertainty of ±2% and peak values in winter (mainly snow and shading effect due to nearby obstacles). Likewise, the energy production of *GMPV* system was studied for more than two years: an enough negative deviation occurs (-10% with uncertainty ≈±1%).

D. Measurements of I-V Curves on PV Arrays

In the presence of noticeable deviation from simulated productivity, the procedure requires to test each array of PV system. The automatic data acquisition system, described in [6], is periodically calibrated and is made of:

- PC notebook and data acquisition device, equipped with one A/D converter (successive approximation, 16 bit-resolution and maximum sampling rate of 1.25 MSa/s) and multiplexer for eight differential channels;
- 3 voltage differential probes, peak values of ±1000 V_{pk};
- 3 current probes (Hall effect), for DC/AC, peak values of ±30-200-2000 A_{pk};
- 1 secondary standard pyranometer, 3 irradiance sensors in m-Si and p-Si silicon and 2 thermometer/anemometer for ambient temperature and wind speed.

The I-V curves of a PV array was measured with a capacitive load, detecting simultaneously voltage, current, irradiance and temperature [16],[17]. The next data-processing to achieve the Standard Test Conditions (*STC*, G=1 kW/m^2, T_c=25 °C) parameters is performed by a conventional correction method [18]. The measurement uncertainties are summarized below.

- for the irradiance G the absolute uncertainty is ±20 W/m^2, for the ambient temperature T_a the absolute uncertainty is ± 0.2 °C, for the cell temperature T_C the absolute uncertainty is ± 2 °C (indirect measurement according to [6],[19] with open circuit voltage and its thermal coefficient);
- for the short circuit current I_{sc}, the open-circuit voltage V_{oc} and the maximum power P_M of the PV generator, the corresponding relative uncertainties are ± 1%, ± 0.1% and ± 1.1%;
- for the fill factor *FF*, defined as the ratio of the maximum power P_M to the product $V_{oc}{\cdot}I_{sc}$, the uncertainty is ± 2%);
- for the maximum power at standard test conditions $P_{mpp} = V_{mpp}{\cdot}I_{mpp}$ (*STC*), the measurement uncertainty is ± 3.5%).

Dust and soiling on PV modules are common factors that contribute to energy losses. In the *BIPV* case-study, during the factory processing, there is air release of substances creating a sticky layer on

the PV modules. Then, organic waste remains long time near the buildings attracting birds with their dropping. To assess the impact of resulting dirt, a mechanical cleaning on two BIPV arrays (225 and 222.5 kWp) was carried out and proper tests were performed before and after the cleaning. Before the cleaning, the power loss was 25% (on one array in Table III and Fig. 5); after the cleaning, the loss was 21%, with a power recovery of 4%. This loss takes into account the power reduction due to the accumulation of dirt, but not the presence of bird dropping which is continuous but non-homogeneous (included into η_{array}). Further tests were performed on 12 arrays to estimate, in average, the other losses: the negative deviations of the measured P_{mpp}, vs. the nameplate data, were >20% in average. It is interesting the inverse relationship of fill factor with power deviations vs. datasheet: low values of *FF* (63—67%) correspond to high deviations vs. datasheet [6].

Other tests were performed on 7 arrays of *GMPV* system with peak power from 48.4 to 55.7 kWp. The *FF* was within 58—65%, but it is corresponding to ambient temperatures higher than in the *BIPV* system. Negative power deviations vs. the nameplate data were in the range from 8—21%, as e.g. shown in Table IV.

According to [7], an 8%-non-thermal losses (η_{array} =92%), although not advisable, is acceptable. In details, the measurements of *I-V* curve at PV-array level include: the Joule losses inside wires and protections; the losses due to the reflection of PV module glasses; the losses consequent to the reduced optical transmittance for dirt. Hence, additional power losses for the *BIPV* system are ≈12%, whereas for the *GMPV* system additional losses are ≈10%.

E. I-V Curves Measurements on PV Strings and Modules

How much is the impact of the mismatch losses? A general answer is hard, it is needed to deepen the analysis case by case. The *BIPV* system, for the reduced supply of components at the moment of installation, was assembled with PV modules strongly affected by *I-V* mismatch. As already said, additional losses were ≈-11% for 14 arrays. Are they caused by the *I-V* mismatch? Hence, it is advisable to proceed from top to down toward the module level, passing through the string level.

Considering one of the greatest PV arrays with 225 kWp, Fig. 6 shows the frequency distribution of 90 string currents at $G \approx 950$ W/m^2 from the on-site monitoring system of the *BIPV* plant during its MPPT operation. It is clear that the current deviations are very wide, putting into evidence the importance of *I-V* mismatch. For the experimental tests, six PV strings were selected, with 50% being the worst strings and 50% being among the better strings in terms of current. Powers P_{mpp}, corrected at STC, were in the range 1.9—2.2 kW (in average 2.1 kW) and their summation (six strings) was 12.2 kW. The results were very interesting, because the voltages at P_{mpp} of the 6 strings are enough different each other (403 V to 457 V), whereas the voltage at maximum power of the PV array is located in intermediate position (443 V).

Really, it is useful to evaluate the impact of the *I-V* curve nonlinearity by comparison with the linear electric circuit theory. At this aim, the Thévenin theorem can be applied, replacing the *I-V* curve of each PV string with a straight line, i.e., the derivative in its own P_M, in which each *k-th* voltage source imposes $2V_{mpp,k}$ and the equivalent resistance is equal to the ratio $V_{mpp,k}/I_{mpp,k}$. Obviously, the *P-V* curve, in this case, becomes a parabola. The calculation of P_M of the 6 strings in parallel is < the summation of the six $P_{M,k}$ with the assumption of stand-alone operation for each string. In other words, the impact of *I-V* mismatch in the parallel connected strings, $\ell_{mis} = 0.2\%$, is negligible if the *I-V* curves are linear. On the other hand, after interpolation of the *I-V* points, in such a way as to have the same voltage values for summing up the currents of the six PV strings, the nonlinear *I-V* characteristic of the parallel is obtained. The resulting P_M on the *I-V* curve is 2% lower than the summation of the six maximum powers (i.e., $\ell_{mis} = 2\%$).

A theoretical model with a 4-parameter equivalent circuit of solar cell [11], was used to quantify the impact of *I-V* mismatch with 90 strings. In this simplified frame, in which a string is made of identical cells, the parameters were: the photovoltaic current I_{ph}; the diode quality factor m; the dark saturation current I_0; the shunt resistance R_{sh}. The series resistance R_s is missing (without loss of generality) to make the *I-V* curve explicit, according to:

$$I = I_{ph} - I_0 \cdot \left(\exp\left(\frac{q \cdot V}{m \cdot k \cdot T \cdot N_c \cdot N_s} \right) - 1 \right) - \frac{V}{R_{sh} \cdot N_c \cdot N_s} \quad (4)$$

the number of cells in a module N_c and the number of series modules in a string N_s are included in the model, where the physical constants are q (electron charge) and k (Boltzmann constant). In such a way, it is easy to construct the parallel of *I-V* curves by summing the string currents for a known value of voltage. The *I-V* mismatch is implemented by the deviations of the four parameters in the ranges I_{ph} =[4.3—5 A]; m =[1.41—1.56]; I_0 =[1—5 μA]; R_{sh} =[1—3 Ω]. The *I-V* curves of 90 different strings and the global array are generated by a proper random function with a distribution of voltage at $P_{M,k}$ in the range [402—492 V]. It is worth noting that the superior limit (492 V) is higher than the measurement, since the simulation does not include the series resistance and the consequent voltage drop in the solar cell circuit. The main results were: the power summation of 900 PV modules $\sum_{k=1}^{90}\left(P_{M,k}\right) = 178.8\ kW$; the array maximum power $P_{M,array}$ =171.4 kW (vs. the measurement P_{mpp} =168.5 kW); voltage =437 V at $P_{M,array}$ (instead of 443 V); consequently, *I-V* mismatch losses $\ell_{mis} = 4\%$.

Thus, the value of $\ell_{mis} = 2\%$ with 6 strings from measurements and the value of $\ell_{mis} = 4\%$ with 90 strings from a theoretical model demonstrate that the *I-V* mismatch losses increase as a function of the number of parallel connected strings.

Going to the module level, 10 m-Si modules, taken from different arrays of the *BIPV* system, were tested (Table V).

The experimental deviations vs. the nameplate data (240 and 250 Wp) are within [-9;-14%]: they are caused by spreads in both current ΔI_{mpp} and voltage ΔV_{mpp}. The deviations of current at P_M, ΔI_{mpp} =[-2%;-13%], put into evidence the presence of *I-V* mismatch when the PV modules were connected in series to form the strings. To evaluate the impact of *I-V* mismatch in a string of 10 modules, a 4-parameter equivalent circuit of solar cell was used, in which a module is made of identical cells. In this case R_s is included and R_{sh} is missing to make the *I-V* curve explicit.

$$V = \frac{m \cdot k \cdot T \cdot N_c}{q} \cdot \ln\left(\frac{I_{ph} - I}{I_0} + 1\right) - N_c \cdot R_s \cdot I \qquad (5)$$

The deviations of the four parameters in (5) are in the ranges I_{ph} =[4.65—5.25 A]; m =[1.45—1.55]; I_0 =[0.5—1 μA]; R_s =[7—14 mΩ]. Thus, the *I-V* curve of the modules is characterized by ΔI_{mpp} =[-2%;-13%], as found in the module testing. The action of bypass diodes was taken into account as a voltage drop of -2.4 V in reverse voltage: 4 diodes per each module. In fact, they are parallel connected across the terminals of 24-cells groups in the *BIPV* system. The connection of one to four weakest modules, i.e., ΔI_{mpp} ≈-13%, generates a range of $\ell_{mis} = 2 - 2.5\%$. The current at P_M of the resulting string is lower than the short circuit current of the weakest modules and thus their bypass diodes are not activated (Fig. 8).

Then, the *I-V* mismatch increases when the strings are connected in parallel, because the strings operate at a global voltage (of the array) different from their voltage at P_M (Fig. 7). These additional losses, caused by interaction of series and parallel connections, and the deviations vs. datasheet (i.e., a power derating) provide 3.5—4% losses. All these mismatch losses contribute a total of 10—11% losses for the *BIPV* system.

F. Advanced Diagnostic Techniques

The EL technique was applied to the set of 10 m-Si modules (Table V), installed 3.5 years before in the *BIPV* system. Eighty-four solar cells, ≈9% of the total number of inspected cells, were defective. A classification of the various crack patterns depending on the reason causing damage can be made according to the prescriptions in [20]. Defective cells, originated from the module production stage, were 9 (11% of the total defective cells in Table VI) and occurred during the firing process of solar cells. This leaded either to temperature inhomogeneities, giving rise to a gradient of the contact resistance of the cell-finger metallization from the cell center to its border (Fig. 9a), or typical chain patterns (Fig. 9b).

In few cases, defective solar cells with interrupted fingers were observed (Fig. 10), although the impact of this type of defect is usually marginal and it does not substantially degrade with time, so that they are not considered in the present statistics.

Defective cells, generated during the assembling of the module components, were 9 (11% of the total defective cells) and mainly regard cracks parallel to busbars caused by soldering of the busbars to the silicon cells (Fig. 11a) or by a lack of connection between one or even two busbars to the cells (Fig. 11b).

Cracked cells, due to transportation and installation, were very frequent (59 cells, corresponding to 70% of the total defective cells). Some of them (35 cells, 42%) already presented electrically inactive areas (Fig. 12a), whereas the remainder (24 cells, 28%) presented cracks still partially conducting (Fig. 12b). Such cracks are very harmful, since their electric resistance may increase under the action of mechanical loading and degrade with time due to thermoelastic effects [21-23].

Finally, 7 cracked cells, 8% of the total defective cells, due to impacts (hail or accidental impacts after installation) were noticed for the pattern of branching cracks (Fig. 13).

Cracks monitored using the EL test are also observable by naked eyes under the appearance of snail tracks in the encapsulant, as shown in Fig. 14.

Since the tested modules exhibited a simultaneous combination of the above types of cracks, it is very difficult to quantify the impact of each typology on the global power losses. Nevertheless, a fair good correlation between the shape of the probability density function (pdf) of the EL intensity of the PV modules and the measured electrical power losses was noticed. In general, the pdf of a module with higher power losses shifts to the left towards lower EL intensities (darker image), as shown in Fig. 15 vs. Table V. It is worth noting that the peaks corresponding to EL intensity ≈ 75 are not an indicator of cracking, since their amplitude is mainly caused by the black pixels (at the four corners of the EL images) around the pseudo-square m-Si cells.

Regarding the same *BIPV* system, the high occurrence of cracks was noticed not only in m-Si modules, but also in p-Si modules (Fig. 16).

EL analysis of a set of m-Si/p-Si modules, belonging to the *GMPV* system, demonstrated significant defects, mostly due to high PID sensitivity and cracking, as discussed in the technical report [24]. PID of ground mounted modules, the closest to the soil, appears frequently and implies defective cells along the frame (Fig. 17). A careful examination of the data reported in [6] permit clarifying the correlation between power loss and cracking in modules affected by the simultaneous presence of PID and cracks. In general, the two phenomena have a similar impact regarding the power losses and therefore a clear trend between number of observed cells and the power losses cannot be deduced.

G. Measurements of the Main PCU Operating Parameters

Concerning the performance of PCUs [25], a multi-hour monitoring of two MPPT and DC-AC converters was carried out. The 2-wattmeter method with voltmeter, ammeter and wattmeter channels is employed [26], for studying the behavior of a three-phase PCU. One of the MPPT racks (S_{rated} =55 kVA) with the DC-AC converter, in the *GMPV* system and one (S_{rated} =125 kVA) among the greatest PCUs in the *BIPV* system provided the following results:

- The MPPT efficiency of the *GMPV* rack is >98% and DC-AC efficiency is >96% from 10% to 80% of power rating with typical values of 99% and 97%, respectively (Fig. 18). Despite a higher power rating, the MPPT efficiency of the *BIPV* inverter is ≈98% and the DC-AC efficiency is always <92%, but the manufacturer datasheets declare 96% as average efficiency.
- Regarding the DC-AC behavior, the losses can be divided mainly into three contributions: the no-load loss (1st); the linear (2nd) and the square loss (3rd) coefficients in percent of the power rating [27]. According to this classification, the *GMPV* rack is characterized by no-load loss of 0.4%, linear coefficient of 0.7% and square coefficient of 3%, whereas the *BIPV* inverter exhibits values of 0.9%, 6% (the highest contribution) and ≈0% for the same parameters.
- The power quality towards the grid [28-30] is acceptable, for all the PCUs, because the power factor *PF* ≈1 and the total harmonic distortion *THD* of current/voltage is <5% close to full load (Fig. 19). The RMS voltage of the grid is not perturbed when the PV input power is close to full

load. Actually, the distribution transformers of the two PV systems are sufficiently oversized to minimize the impact of their short circuit impedance.

4. CONCLUSIONS

A comprehensive power and energy procedure permits to quantify the sources of losses in the two most important grid-connected applications, i.e., the ground-mounted and the building-integrated PV systems. Here, two case studies are analyzed, in which the performance in energy production is particularly poor to highlight the procedure effectiveness. The main source of additional losses, vs. the reference production, is the *I-V* mismatch accounting for, at least, ≈6.5% in the *BIPV* system. It includes the contributions of parallel and series connections, calculated separately through theoretical models. The interaction of series and parallel mismatch provides a further amount of losses which, together with the checked power derating of PV modules, justifies 3.5—4.5% losses. The mean losses for dirt and shade provide 4—6%, while the remaining losses (4%) are due to the PCUs with low frequency transformer. Thanks to electroluminescence, it was highlighted that, in the *BIPV* system, the *I-V* mismatch was a consequence of poor quality inspection in the PV-module manufacturing, in terms of both mechanical defects and lack of sorting. The breakage of solar cells was demonstrated, due to installation and maintenance phases. In the *GMPV* system, the potential induced degradation with the consequent *I-V* mismatch and power derating was observed (10% of additional losses), because of some PV modules were placed very close to the ground with noticeable humidity.

As a further finding, the dirt has a sensible impact in the case of PV system located in a food/pharmaceutical factory. Then, the power losses in *MPPT* and DC-AC conversions were higher than those declared by the manufacturer of PCUs with 50-Hz transformer. Finally, as a solution or mitigation of the underperformance, it is possible the replacement of PV modules and inverters at their current prices (<1 €/Wp). This is true taking into account the generous rates (0.3—0.45 €/kWh) of the old feed-in tariffs in Italy.

ACKNOWLEDGEMENTS

M. Paggi would like to acknowledge the European Research Council for supporting the ERC Grant Agreement No. 306622 (ERC Starting Grant "Multi-field and multi-scale Computational Approach to Design and Durability of PhotoVoltaic Modules" – CA2PVM) within the European Union's Seventh Framework Programme (FP/2007–2013). The authors from the Department of Structural, Geotechnical and Building Engineering of Politecnico di Torino would like to thank the support of the Italian Ministry of Education, University and Research to the Project FIRB 2010 Future in Research "Structural mechanics models for renewable energy applications" (RBFR107AKG)

REFERENCES

[1] *Italian Law, number 116, 11th August 2014* link to http://www.gazzettaufficiale.it/eli/id/2014/08/20/14G00128/sg.

[2] G. Chicco, F. Corona, R. Porumb, F. Spertino, "Experimental Indicators of Current Unbalance in Building-Integrated Photovoltaic Systems," *IEEE Journal of Photovoltaics*, vol.4, pp.924-934, May 2014.

[3] A. Ndiaye, A. Charki, A. Kobi, C. M. Kébé, P. A. Ndiaye, V. Sambou, Degradations of silicon photovoltaic modules: A literature review, *Solar Energy*, Vol. 96, 2013, pp. 140-151.

[4] *Grid connected photovoltaic systems-minimum requirements for system documentation, commissioning test and inspection*, IEC Standard 62446, 1st edition 2009.

[5] J.V. Muñoz, G. Nofuentes, J. Aguilera, M. Fuentes, P.G. Vidal, "Procedure to carry out quality checks in photovoltaic grid-connected systems: Six cases of study," *Applied Energy*, vol. 88, 2011, pp. 2863-2870.

[6] F. Spertino, A. Ciocia, F. Corona, P. Di Leo, F. Papandrea, "An experimental procedure to check the performance degradation on-site in grid-connected photovoltaic systems," *40th IEEE Photovoltaic Specialists Conference (PVSC)*, pp. 2600-2604, 2014.

[7] *Guide for design and installation of photovoltaic (PV) systems connected to MV and LV networks*, CEI Standard 82-25, 2010 (in Italian).

[8] *Photovoltaic system performance monitoring, Guidelines for measurement, data exchange and analysis*, IEC Standard 1724, 1998.

[9] *Photovoltaic systems-Power Conditioners, Procedure for measuring efficiency*, IEC Standard 61683, 1999.

[10] J. Muñoz, F. Martinez-Moreno, E. Lorenzo, "On-site characterization and energy efficiency of grid-connected PV inverters," *Progress in Photovoltaics: Research and Applications*, vol. 19, 2011, pp. 192–201.

[11] F. Spertino, J.S. Akilimali, “Are manufacturing I-V mismatch and reverse currents key factors in large photovoltaic arrays?,” *IEEE Transactions on Industrial Electronics*, vol. 56, 2009, pp. 4520-4531.

[12] JRC, Free Online Estimation of the Solar Irradiance and Ambient Temperature, [European Commission Online]. Available: http://re.jrc.ec.europa.eu/pvgis

[13] F. Spertino, F. Corona, “Monitoring and checking of performance in photovoltaic plants: A tool for design, installation and maintenance of grid-connected systems,” *Renewable Energy*, vol. 60, Dec. 2013, pp. 722-732.

[14] *Energia solare. Calcolo degli apporti per applicazioni in edilizia. Valutazione dell’energia raggiante ricevuta*, Italian Standard UNI 8477, 1983.

[15] B.Y. Liu, R.C. Jordan, “The interrelationship and characteristic distribution of direct, diffuse and total solar radiation,” *Solar Energy*, vol. 4, 1960, pp. 1-19.

[16] F. Spertino, J. Sumaili, H. Andrei, G. Chicco, “PV module parameter characterization from the transient charge of an external capacitor,” *IEEE Journal of Photovoltaics*, vol. 3, 2013, pp. 1325-1333.

[17] F. Attivissimo, F. Adamo, A. Carullo, A. M. Lanzolla, F. Spertino, A. Vallan, “On the performance of the double-diode model in estimating the maximum power point for different photovoltaic technologies,” *Measurement*, vol. 46, 2013, pp. 3549-3559.

[18] *IEC Standard 60891, 2009, Photovoltaic Devices – Procedures for Temperature and Irradiance Corrections to Measured I-V Characteristics.*

[19] *EN Standard 61829, 1998, Crystalline silicon photovoltaic (PV) array: on-site measurement of I-V characteristics.*

[20] IEA-PVPS T13-01:2014. “Review of Failures of Photovoltaic Modules”, 2014, ISBN 978-3-906042-16-9.

[21] M. Paggi, I. Berardone, A. Infuso, M. Corrado, “Fatigue degradation and electric recovery in Silicon solar cells embedded in photovoltaic modules,” *Scientific Reports*, vol. 4, 2014, art. 4506.

[22] I. Berardone, M. Corrado, M. Paggi, “A generalized electric model for mono and polycrystalline silicon in the presence of cracks and random defects,” *Energy Procedia*, vol. 55, 2014, pp. 22-29.

[23] J. Käsewieter, F. Haase, M. Haro Larrodé, M. Köntges, “Cracks in solar cell metallization leading to module power loss under mechanical loads,” *Energy Procedia*, vol. 55, 2014, pp. 469-477.

[24] PI, Photovoltaik-Institut, Berlin AG, Document on investigation of commercial modules with focus on potential induced degradation, 2013.

[25] A. Woyte, J. Nijs, R. Belmans, Partial shadowing of photovoltaic arrays with different system configurations: literature review and field test results, *Solar Energy*, vol. 74, 2003, pp 217-233, http://dx.doi.org/10.1016/S0038-092X(03)00155-5.

[26] F. Spertino, G. Graditi, “Power conditioning units in grid-connected photovoltaic systems: a comparison with different technologies and wide range of power ratings,” *Solar Energy*, vol. 108, 2014, pp. 219-229.

[27] F. Spertino, F. Corona, P. Di Leo, “Limits of advisability for master-slave configuration of DC-AC converters in photovoltaic systems,” *IEEE Journal of Photovoltaics*, vol. 2, 2012, pp. 547-554.

[28] G. Chicco, R. Napoli, F. Spertino, "Experimental evaluation of the performance of grid-connected photovoltaic systems," *Electrotechnical Conference, 2004. MELECON 2004. Proceedings of the 12th IEEE Mediterranean*, vol. 3, 12-15 May 2004, pp.1011-1016.

[29] F. Batrinu, G. Chicco, J. Schlabbach, F. Spertino, "Impacts of grid-connected photovoltaic plant operation on the harmonic distortion," *Electrotechnical Conference, 2006. IEEE MELECON 2006*, 16-19 May 2006, pp.861-864.

[30] Yang Du, Dylan Dah-Chuan Lu, Geoffrey James, David J. Cornforth, Modeling and analysis of current harmonic distortion from grid connected PV inverters under different operating conditions, Solar Energy, vol. 94, August 2013, pp. 182-194, http://dx.doi.org/10.1016/j.solener.2013.05.010.

Fig. 1. Photo of two successive rows of PV modules in the *GMPV* system.

Fig. 2. Satellite image of the 2.5 MWp *BIPV* system.

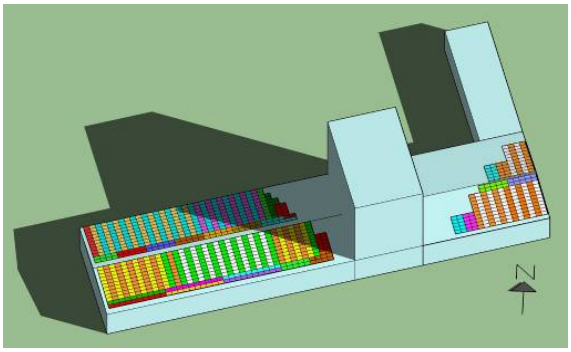

Fig. 3. Simulation of shadows on the closest PV strings (10:30 am in spring).

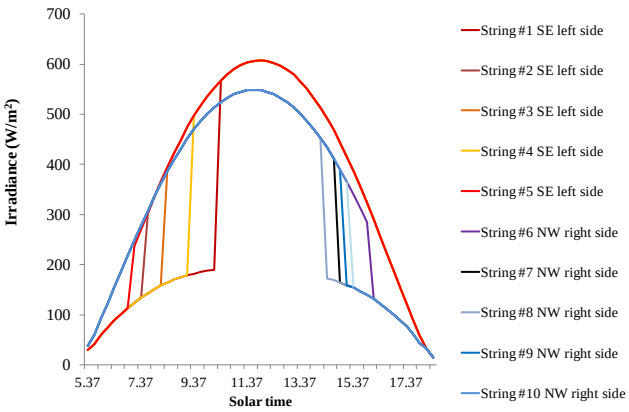

Fig. 4. Global irradiance and diffuse contribution in spring on 10 strings.

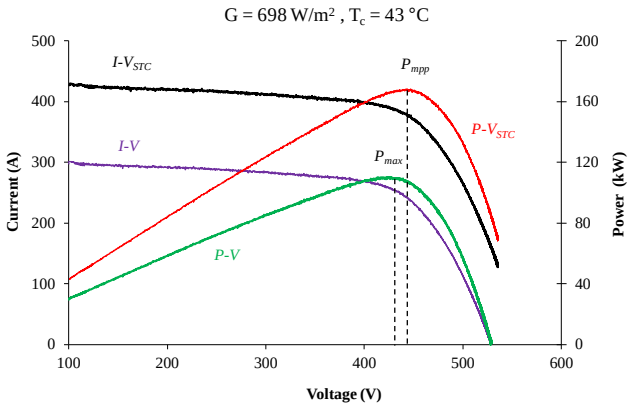

Fig. 5. The I-V and P-V curves of a dirt array at real and STC conditions.

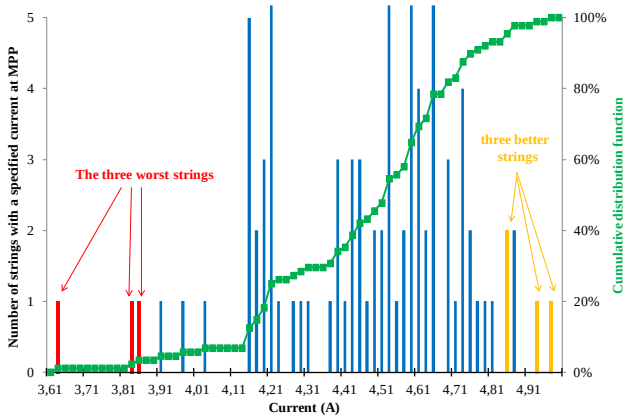

Fig. 6. Current distribution of the 90 strings in operating conditions.

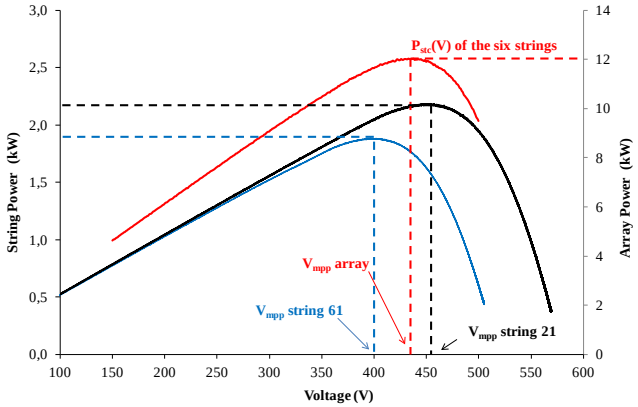

Fig. 7. P-V curves of the best string, the worst string (as current production) and the whole array.

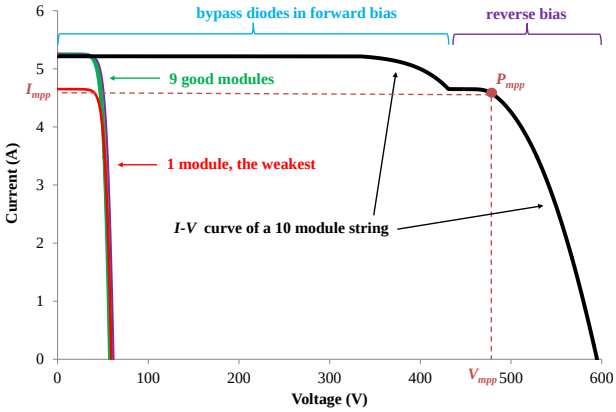

Fig. 8. Simulation of string *I-V* curve with current deviation at maximum power due to mismatch.

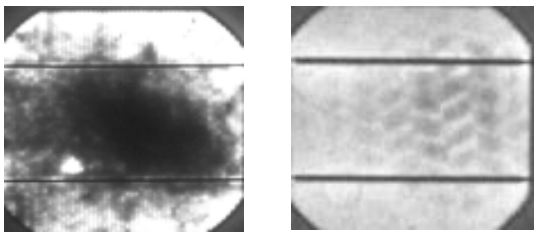

(a) Non-uniform contact resistance (b) Chain pattern

Fig. 9. EL images of solar cells with problems originated during firing.

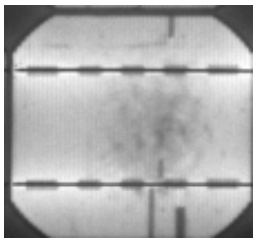

Fig. 10. EL image of a defective solar cell with broken fingers.

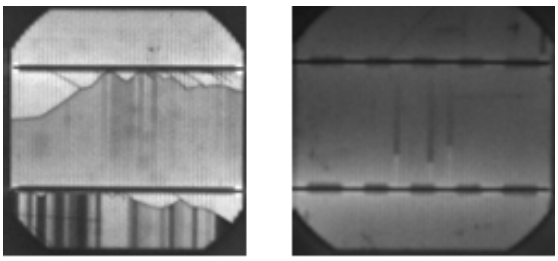

(a) Cracks due to soldering (b) One busbar disconnected

Fig. 11. EL images of cells with problems during module assembling.

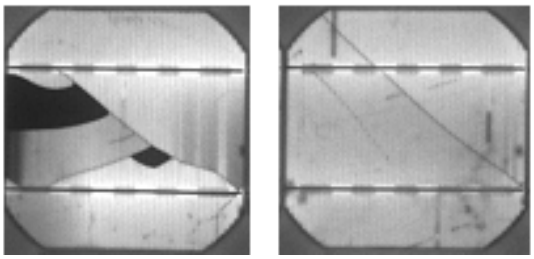

(a) Electrically insulated cracks (b) Electrically conductive cracks

Fig. 12. EL images of cells with cracks during transportation and installation.

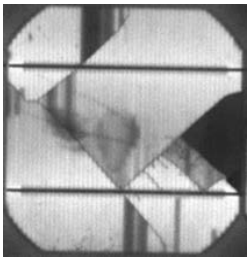

Fig. 13. EL images of solar cells with cracks due to impacts.

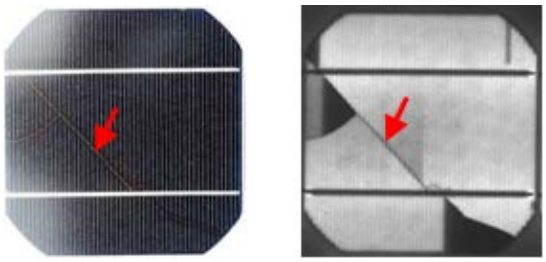

Fig. 14. Visual inspection of a cell (left) with snail tracks in correspondence of cracks detected by EL (right).

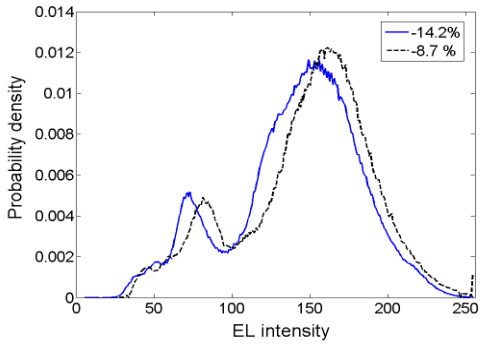

Fig. 15. Correlation between probability density function of the EL intensity signal and the module power loss.

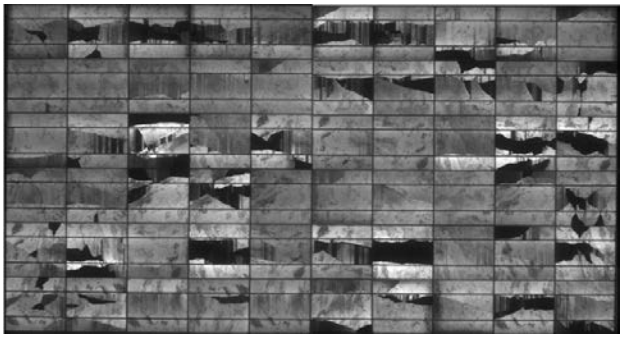

Fig. 16. EL image of a 60 p-Si cell module with high occurrence of cracks.

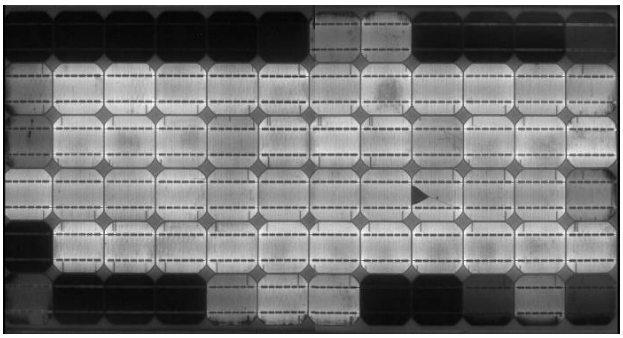

Fig. 17. EL image of a 72 m-Si cell module affected by PID.

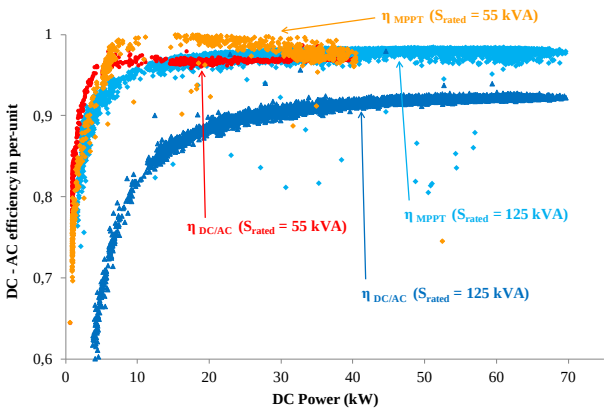

Fig. 18. MPPT and DC-AC efficiencies of *GMPV* and *BIPV* inverters.

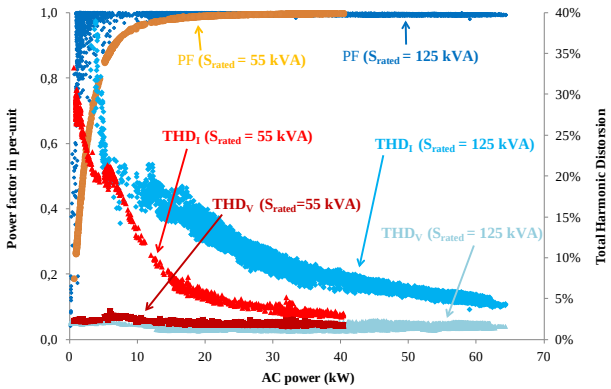

Fig. 19. Power factor and total harmonic distortion of current/voltage in *GMPV* and *BIPV* inverters.

TABLE I Monthly Energy Results of *BIPV* System in kWh

Month	From prediction	From energy counter	Deviation
Jan	99839	44551	-55%
Feb	131413	71370	-46%
Mar	170039	133661	-21%
Apr	217292	183283	-16%
May	320607	263751	-18%
Jun	353619	307208	-13%
Jul	338568	293954	-13%
Aug	308895	267920	-13%
Sep	267043	210297	-21%
Oct	153712	123702	-20%
Nov	106886	73571	-31%
Dec	95065	59854	-37%
Total	2562980	2033122	-20%

TABLE II Yearly Performance Parameters of *BIPV* System

Reference Yield	Predict. Final Yield	Monit.Final Yield	Predict.Perf. Ratio	Monit.Perf. Ratio
Y_r (h/y)	Y_f (h/y)	Y_f (h/y)	R_p	R_p
1452	1132	913	78%	63%

TABLE III Power Results on a PV Array of the *BIPV* System

Item	Test1	Test2	Test3	AVG	
T_a	16.8	17.1	17.5	17.2	°C
G	698	697	698	698	W/m^2
T_c	43.0	43.0	43.0	43.0	°C
P_M	109.3	109.5	109.2	109.4	kW
V_{Pmax}	426.9	423.0	424.1	424.6	V
V_{oc}	530.1	529.7	529.4	529.5	V
I_{Pmax}	256.1	258.9	257.4	257.7	A
I_{sc}	306.1	304.6	305.7	305.3	A
FF	67.4%	67.9%	67.5%	67.7%	
Parameters at *STC*					
P_{mpp}	168.5	169.0	168.1	168.5	kW
V_{mpp}	440.9	440.6	444.3	443.2	V
I_{mpp}	382.3	383.5	378.4	380.2	A
Deviation vs. datasheet	-25.1%	-24.9%	-25.3%	-25.1%	
ΔI_{mpp}	-14.0%	-13.7%	-14.9%	-14.5%	
ΔV_{mpp}	-12.9%	-12.9%	-12.2%	-12.4%	

TABLE IV Power Results on a PV Array of the *GMPV* System

Item	Test1	Test2	Test3	AVG	
T_a	31.0	30.8	30.4	30.7	°C
G	980	993	994	989	W/m^2
T_c	61.6	61.8	61.5	61.6	°C
P_M	38.25	38.96	39.86	39.03	kW
V_{Pmax}	514.2	516.4	518.4	516.4	V
V_{oc}	726.7	727.9	732.9	729.2	V
I_{Pmax}	74.4	75.4	76.9	75.6	A
I_{sc}	91.0	92.4	92.0	91.8	A
FF	57.9%	57.9%	59.1%	58.3%	
Parameters at *STC*					
P_{mpp}	46.56	46.98	47.72	47.09	kW
V_{mpp}	612.99	617.47	607.96	612.81	V
I_{mpp}	75.95	76.09	78.48	76.84	A
Deviation vs. datasheet	-16.4%	-15.6%	-14.3%	-15.4%	
ΔI_{mpp}	-10.1%	-9.9%	-7.1%	-9.0%	
ΔV_{mpp}	-6.8%	-6.1%	-7.6%	-6.8%	

TABLE V Test Results on ten PV modules of the *BIPV* System

	P_{mpp} (*STC*)	V_{mpp} (*STC*)	I_{mpp} (*STC*)	Deviation vs. datasheet	ΔI_{mpp} (*STC*)	ΔV_{mpp} (*STC*)
	(W)	(V)	(A)			
Mod#1	218	46.89	4.64	-12.9%	-6.0%	-7.3%
Mod#2	214	46.18	4.64	-14.2%	-6.0%	-8.7%
Mod#3	216	47.01	4.58	-13.8%	-7.2%	-7.1%
Mod#4	218	46.54	4.67	-13.0%	-5.4%	-8.0%
Mod#5	215	46.67	4.60	-10.6%	-3.6%	-7.2%
Mod#6	224	47.36	4.72	-10.5%	-4.0%	-6.7%
Mod#7	221	47.42	4.66	-11.7%	-5.3%	-6.6%
Mod#8	228	47.44	4.81	-8.7%	-2.3%	-6.6%
Mod#9	217	47.02	4.62	-13.1%	-12.8%	-0.4%
Mod#10	225	47.93	4.70	-9.9%	-4.5%	-5.6%

TABLE VI Summary of EL Results on Defective m-Si Modules

Origin of defect	Freq. of occurrence
Defects originated during firing	11%
Defects originated during module assembling	11%
Cracks due to transport or installation (already contributing to power losses)	42%
Cracks due to transport or installation (not yet contributing to power losses)	28%
Cracks due to impacts (hail or accidental impacts)	8%